2013 IEEE/RSJ International Conference on
Intelligent Robots and Systems (IROS)
November 3-7, 2013. Tokyo, Japan

A Novel Flexure-based Dual-arm Robotic System for High-throughput Biomanipulations on Micro-fluidic Chip

Hui Tang, Yangmin Li*, *Senior Member*, IEEE, and Xiao Xiao

***Abstract*— In recent years, robotic bio-manipulation emerges as a hot research topic in the micro/nano technology. In these applications, biological cell microinjection is a focus since it is a critical process for the further biological research such as genetic engineering and pharmacology research. This study aims to develop a novel robotic biomanipulation system combining with the micro-fluidic chip technology to improve the cell manipulation stability and throughput. Two novel flexure-based large-workspace micromanipulators with modified differential lever displacement amplifier (MDLDA) are presented in this paper. After a series of optimal designs and mechanism modeling, the mechanism performances are evaluated by the FEA method. Finally, the proposed micromanipulators are fabricated and visual-servo controlled to perform the practical zebrafish embryos injection task. In this work, two piezoelectric (PZT) actuators P-216.80 (open-loop travel is 120 μm) and one PZT actuator P-840.20 (open-loop travel is 30 μm) are utilized in the compliant mechanisms, the experiment results indicate that the displacement amplification ratios can reach up to 30.6 and 17.6, thus the maximum output displacements can achieve around 3.1273 mm and 0.528 mm, the rotation angle of the left micromanipulator can reach to around 26.5°. Both theoretical derivation and experimental implementation results well verify the advanced performance of the developed system.**

I. Introduction

Development of biomedical technology in the past decades was fast and fruitful, which made them possible to operate biological cells or even bacteria in micro world. In these applications, biological cell microinjection is a focus since it is a critical process for conducting the further cell research such as genetic engineering and pharmacology research [1, 2]. However, how to perform this task in a reliable, high-throughput, and easy manner is not an easy work. Conventional methods of the cell microinjection process can mainly be realized by the technican. However, not to mention these methods have the problems of low success rate, visual fatigue, and low positioning precision, a tiny shake operation may cause serious damage to the cell due to the fragility and slippery feature of the membrane.

In order to cater to this requirement, many research groups have focused on the robotic cell micromanipulation technologies [3]. However, these devices and technologies can not fulfill the tasks well in the case of higher throughput, smaller sample volume, and higher manipulation precision. With these considerations, robotic biomanipulation combining with the micro-fluidic chip technology emerges as a novel method to solve this problem. Previous works dedicated to biological micromanipulations on chip are pioneered in [4–6]. In these works, the microrobots on microfluidic chip are driven by the non-contact magnetic forces generated by the horizontally arranged permanent magnets, however, the defect of low operation accuracy is a bottleneck, which should be resolved.

In order to enhance the robotic system precision, all the factors should be taken into the consideration, while the first issue is the positioning precision of the micro/nano manipulator. Therefore, a set of novel piezoelectric (PZT) actuated flexure-based large-workspace micromanipulators with MDLDA is proposed in this paper. As we known, the advantages of compliant mechanism can be concluded as follows: reduced cost, easy to fabricate, no friction, and ultra-high motion precision. Besides, with comparisons to the other actuators such as thermal and electrostatic actuators, PZT actuator possesses the advantages of larger blocking force and quicker response speed.

In the past few years, some flexure-based compliant micromanipulators have been proposed towards the bio-medical applications, while the defect of small workspace constrains its practical applications. To amplify the output displacement of the PZTs, some mechanical displacement amplifiers are proposed and employed [7, 8]. In these devices, the lever displacement amplifiers have been most widely employed due to its simple mechanism structure, however, the conventional lever mechanism cannot meet the bio-manipulation requirement because of its small amplification ratio. After an elaborate design, a type of modified differential lever displacement amplifier is presented and utilized in this work.

Finally, by means of a series of mechanism optimizations, a prototype is fabricated practically and experimentally tested. Two high-voltage (0-1000 V) driven PZT (P-216.80 from PI, Inc.) with open travel 120 μm and one low-voltage (0-100 V) driven PZT (P-840.20 from PI, Inc.) are employed in this system. The command signal and the output displacement data are generated and captured by the DAQ card (PCI-6289, from NI, Inc.) and the microscopy system (BX51WI, from Olympus, Inc.), respectively. The amplification ratio test results indicate that the displacement amplification ratio of the left and right micromanipulators can reach up to 30.6 and 17.6, respectively, thus the output displacement of the fabricated micromanipulator can achieve

This work was supported in part by National Natural Science Foundation of China (Grant No. 61128008), Macao Science and Technology Development Fund (Grant No. 016/2008/A1), Research Committee of University of Macau under Grant No.:MYRG183(Y1-L3)FST11-LYM and MYRG203(Y1-L4)-FST11-LYM).

H. Tang, Y. Li, and X. Xiao are with the Dept. of Electromech. Engineering, University of Macau, Taipa, Macao SAR, China. Y. Li is also with School of Mechanical Engineering, Tianjin University of Technology, Tianjin 300191, China *Corresponding author: ymli@umac.mo (Yangmin Li)

up to 3.672 mm and 0.528 mm, respectively, the maximum rotation angle can achieve 26.5°. The practical zebrafish embryos injection experiment is successfully conducted by using a PID closed-loop control strategy, which confirms the satisfactory performance of the developed system.

II. Novel Biomanipulation Method Using Flexure-Based Dual-Arm Robotic System

As aforementioned, with the development of biomedical technology, the scholars are devoting to establish an automatic system to perform the cell micromanipulation tasks. In these conventional systems, living cells are suspended in the culture broth, the two micromanipulators are symmetrically installed in the microscope rack, the capillary glass tube grasped by the left micromanipulator will be used to absorb the cells, while the capillary glass micropipette grasped by the right micromanipulator will be used to manipulate the captured cells [9]. It reveals that these systems can not meet the requirements of higher throughput, smaller sample volume, and higher manipulation precision.

To solve these problems, a novel cell micromanipulation system including dual-arm flexure-based micromanipulators is proposed to perform the cell micromanipulation tasks on a micro-fluidic chip. As shown in Fig. 1, the micromanipulation system consists of an up-right microscopy system, a set of dual-arm PZT-driven micromanipulator with short rigid cantilever beams, the two micromanipulators move in $Y\theta$ and Y direction, respectively. Besides, the micro-fluidic chip is mounted on a small stage, which can be adjusted up and down to determine the best position, the two microrobots are designed by using two Ni plates for future cell manipulations. They are driven by the two permanent magnets which are symmetrically positioned on the cantilever beams, as shown in Fig. 2. A big chamber is designed for accommodation of the microrobots. Firstly, the cells are delivered to the loading area, then, the left microrobot with a pocket will grip and transport the cells one by one to the assigned area also, the left microrobot will be employed to roll the cells to an appropriate position, then the right microrobot will perform the microinjection tasks. The injected cells will be transported to an assigned region by the micro-fluid flush force. Finally, these cells will be collected by the micro-well cells culture devices.

In summary, flexure-based robotic cell manipulation on a micro-fluidic chip presents great advantages such as high-precision, non-skill dependent, high reliability and high throughput. Permanent magnetic force is adopted to operate the microrobots due to its non-contact, easy to assemble, and low cost.

III. Flexure-based Micromanipulator Design and Modeling

In this paper, our objective is to design two flexure-based micromanipulators with large-workspace and high motion precision for high performance cell injection on micro-fluidic chip. In view of this, the two micromanipulators should possess large displacement amplification ratio. Then, the design detail is demonstrated as follows.

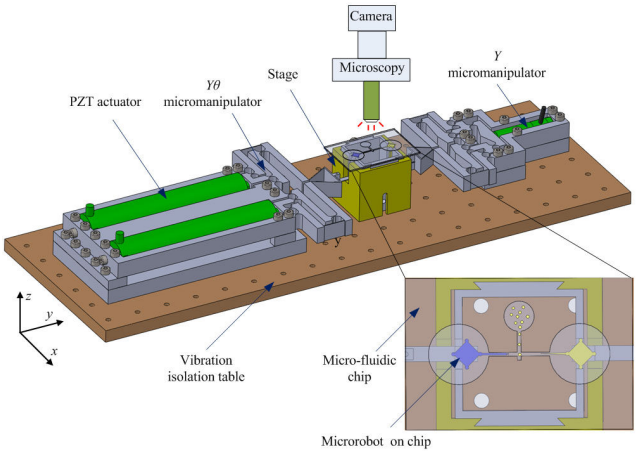

Fig. 1. The dual-arm flexure-based robotic system for bio-manipulation on a micro-fluidic chip.

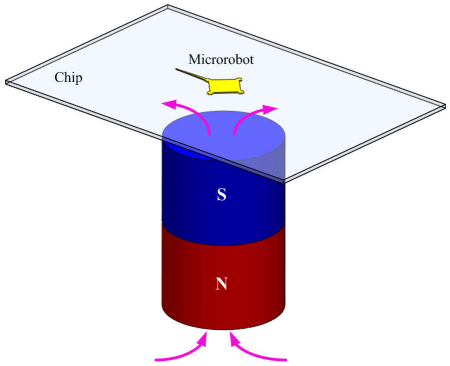

Fig. 2. The schematic of the microbots driven by the permanent magnetic forces.

A. Design of the Micromanipulators with MDLDA

As aforementioned, the short stroke of the PZT actuators is a bottleneck which constrains its further applications, hence adding some mechanical displacement amplifiers along with the PZT actuators is an effective method to enhance the mechanism workspace [10]. In these applications, lever displacement amplifier has been widely employed due to its simple mechanism structure and stable performance. However, the conventional lever displacement cannot be directly employed in this work since its displacement amplification ratio is much small. In this study, a modified differential lever displacement amplifier is designed and it possesses the following advantages: 1) the structure is simple, the size is relatively small; 2) the symmetrical structure, hence it can output high precision motion, since this amplification mechanism possesses integrated high rigidity, therefore, the lateral coupling displacement error of this mechanism will be completely eliminated in theory.

1) Left Micromaniputor Design: In this study, a $Y\theta$ left micromanipulator with MDLDA mechanism is proposed as shown in Fig. 3(a). It is constructed by a pair of symmet-

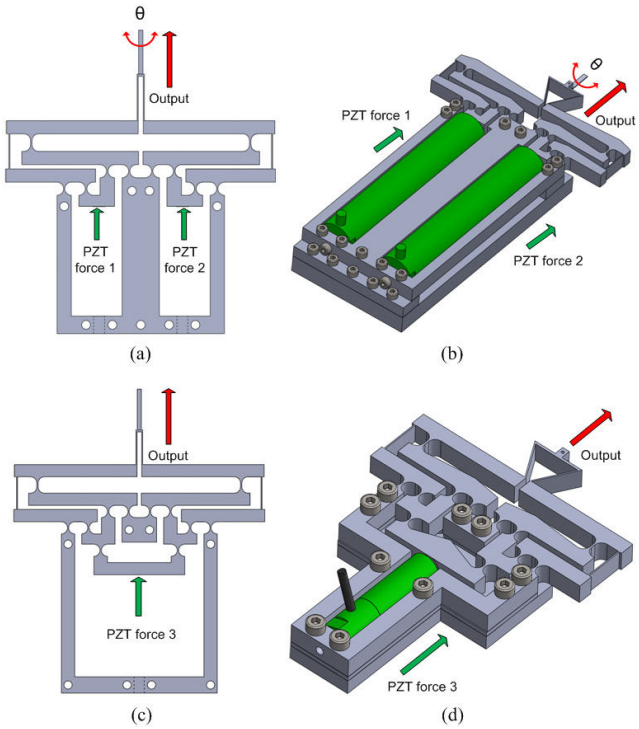

Fig. 3. The proposed flexure-based micromanipulators. (a) Left $Y\theta$ micromanipulator without dimension optimization, (b) After dimension optimization, (c) Right Y micromanipulator without dimension optimization, (d) After dimension optimization.

rically MDLDA mechanisms. The working principle of this micromanipulator is: On one hand, if you need a rotation movement with large motion range, you can exert a voltage at the PZT 1 or PZT 2 according to the practical requirements, then the amplified motions are transferred to the end-effector to perform the cell rolling task. On the other hand, if you need a linear movement with large motion range to perform the inserting task, you can synchronously exert the voltages at the two PZTs. In this study, circular flexure (see Fig. 4(a)) is adopted in the mechanism designs, with the comparisons to the other flexures (e.g Fig. 4(b)), it can output a high precision displacement. Moreover, considering the "displacement loss" effect arising from preload force, the PZTs are immobilized by the screws which can be fine tuned to enhance the motion output capacity of the PZT actuators.

2) Right Micromaniputor Design: Afterwards, a Y right micromanipulator with MDLDA mechanism is proposed as shown in Fig. 3(c). The mechanism structure and working principle is similar to the left micromanipulator, and it can output a high precision linear motion to fulfill the cell manipulation task.

B. Amplification Ratio Determination

In order to let the micromanipulator output a large displacement, the displacement amplification ratio of the employed MDLDA should be modeled to make an optimization. As shown in Fig. 5, a schematic is established to demonstrate the mechanism working principle. According to the lever amplification principle, the output displacement of the

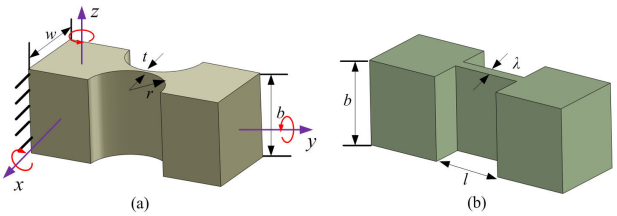

Fig. 4. The circular flexure hinge (a) and the beam flexure hinge (b) with the structure parameters.

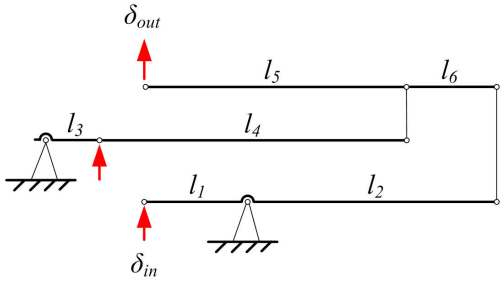

Fig. 5. The schematic of modified differential displacement amplification mechanism.

micromanipulator can be derived as follows:

$$\delta_{out} = \left[\frac{l_5}{l_6}\left(\frac{l_2}{l_1} + \frac{l_4}{l_3} + 1\right) + \frac{l_4}{l_3} + 1\right]\delta_{in} \tag{1}$$

where δ_{in} denotes the input displacement, δ_{out} denotes the output displacement. Then, the displacement amplification ratio will be derived as follows:

$$A = \left[\frac{l_5}{l_6}\left(\frac{l_2}{l_1} + \frac{l_4}{l_3} + 1\right) + \frac{l_4}{l_3} + 1\right] \tag{2}$$

where A is the displacement amplification ratio, and it can be observed that the displacement amplification ratio is determined by the length ratios of the lever arms. In our next section, a series of dimension optimization works will be carried out to enhance the mechanism workspace.

C. Dimension Optimization using PSO Algorithm

In our previous study, it is found that the lever amplification ratio will always be smaller than the theoretical value, which is mainly caused by the lever arm bending and the flexure hinge stretching. Therefore, in this study, the dimension parameters of the flexure hinges will be taken into consideration. This optimization task can be described as follows:

1) Objective: Maximize displacement amplification ratio (A).
2) Related parameters: w, r, t, l, λ, l_1, l_2, l_3, l_4, l_5, l_6.
3) Subject to:
a) Amplification ratio $A_m \geq 10$;
b) Ranges: 4 mm $\leq w \leq$ 8 mm, 2 mm $\leq r \leq$ 5 mm, 0.3 mm $\leq t \leq$ 1 mm, 8 mm $\leq l \leq$ 25 mm, 0.3 mm $\leq \lambda \leq$ 1 mm, 4 mm$\leq l_1 \leq$ 10 mm, 10 mm$\leq l_2 \leq$ 30 mm. 4 mm$\leq l_3 \leq$ 6 mm, 10 mm$\leq l_4 \leq$ 40 mm, 10 mm$\leq l_5 \leq$ 30 mm, 4 mm$\leq l_6 \leq$ 10 mm.

TABLE I

THE PARAMETERS OF THE OPTIMAL LEFT MICROMANIPULATOR

Structural parameters (mm)					
w	r	t	l	λ	l_1
6.65	3	0.65	18	0.5	4
l_2	l_3	l_4	l_5	l_6	
30	6	10	30	4	

TABLE II

THE PARAMETERS OF THE OPTIMAL RIGHT MICROMANIPULATOR

Structural parameters (mm)					
w	r	t	l	λ	l_1
6	2.65	0.6	15	0.5	3.5
l_2	l_3	l_4	l_5	l_6	
26	5	8	25	3.5	

The parameter b is not considered in this optimization work since the thickness of the fabricated material is specified (12 mm). Moreover, the thinnest part of the flexures is no less than 0.3 mm since the stage will be manufactured by WEDM (wire electro-discharge machining) technique which can not ensure a tolerance of $\pm$ 0.01 mm once the thickness is smaller than 0.3 mm. The parameters of $l_1 \sim l_6$ of the displacement amplification levers are optimized to obtain the maximum displacement amplification ratio with a compact structure. After the optimizations based on PSO, the displacement amplification ratio of the left micromanipulator can achieve 33.6, however, the initial displacement amplification ratio is smaller than this value, then the parameters of w, r, t, l, and λ are fine tuned to reduce the lost displacement. According to our previous study, the lever shape is assigned as a wedge to strengthen the lever arm [8].

After several tries, the optimal mechanism parameters are shown in Table I and Table II, the theoretical displacement amplification ratios of the two micromanipulators are 33.6 and 18.1, respectively.

IV. MECHANISM PERFORMANCE EVALUATION VIA FEA

In this section, the optimized mechanism performances are validated by the ANSYS Workbench TM Platform. The FEA test in terms of prismatic motion analysis, stress analysis, displacement amplification ratio analysis, rotation angle analysis, and modal analysis are conducted in detail.

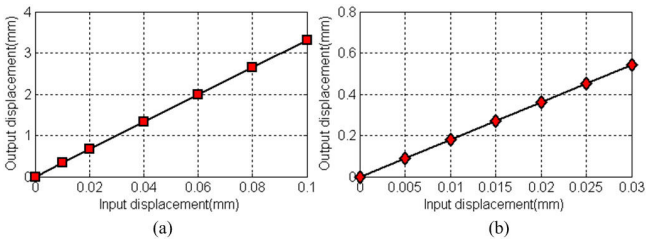

Fig. 6. The relationship between the input displacement and the output displacement of the optimized micromanipulator. (a) Left micromanipulator, (b) Right micromanipulator.

A. Static Structural Analysis

1) Left Micromanipulator Analysis: Firstly, the parasitic rotational yaw has been tested, four symmetric points on the left and right lever arms are specified, it can be derived that the maximum parasitic rotational yaw is less than 0.009 mrad, which proves the well-decoupled property of the proposed mechanism. To test the strain response performance of this mechanism, a set of forces 0$\sim$1800 N are exerted at the two driving points synchronously. It is observed that the relationship between the output displacement and the input force is linear, which reveals that the stiffness nonlinear effect is not appeared in this mechanism. Besides, it exhibits that the developed micromanipulator possesses the potential to bear the input force up to 1800 N, where the maximum von Mises stress is 483.5 MPa without material failure. To test the displacement amplification ratio performance of this mechanism, a set of input displacement 0 μm, 10 μm, 20 μm, 40 μm, 60 μm, 80 μm, and 100 μm are exerted at the two driving points synchronously. As shown in Fig. 6(a) and Fig. 7(a-b), the value of the displacement amplification ratio is not influenced by the input displacement, also, the displacement amplification ratio can be calculated as around 33, thus the maximum output displacement can reach up to 3.1273 mm, which demonstrates that the "displacement loss" effect caused by the lever bending and flexure hinge stretching has been overcome after the mechanism optimization designs. Furthermore, the rotation angle analysis is calculated as around 26.5°.

2) Right Micromanipulator Analysis: The process is similar to the left micromanipulator analysis, the FEA results are: the maximum parasitic rotation yaw is almost zero, the right micromanipulator possesses the potential to bear the input force up to 1200 N, where the maximum von Mises stress is 483.5 MPa without material failure, the displacement amplification ratio can be calculated as around 17.6, thus the maximum output displacement can reach up to 0.528 mm (see Fig. 6(b) and Fig. 7(c-d)).

B. Modal Analysis

Also, the modal analysis is carried out to verify their dynamic performance. It indicates that the proposed left micromanipulator possesses a high working frequency (219.03 Hz), the right micromanipulator possesses a higher working frequency (306.81 Hz). All the results further confirm that the proposed micromanipulation has a high mechanism bandwidth for performing high rate cell manipulations.

V. EXPERIMENTS AND DISCUSSIONS

In this section, the prototypes of the designed compliant micromanipulators are fabricated and experimentally tested to evaluate the system performance.

A. Prototype Fabrication and Experimental Setup

As shown in Fig. 8, the micromanipulators are fabricated by using the WEDM (wire electro-discharge machining) process from a piece of AL7075-T651 material, which has

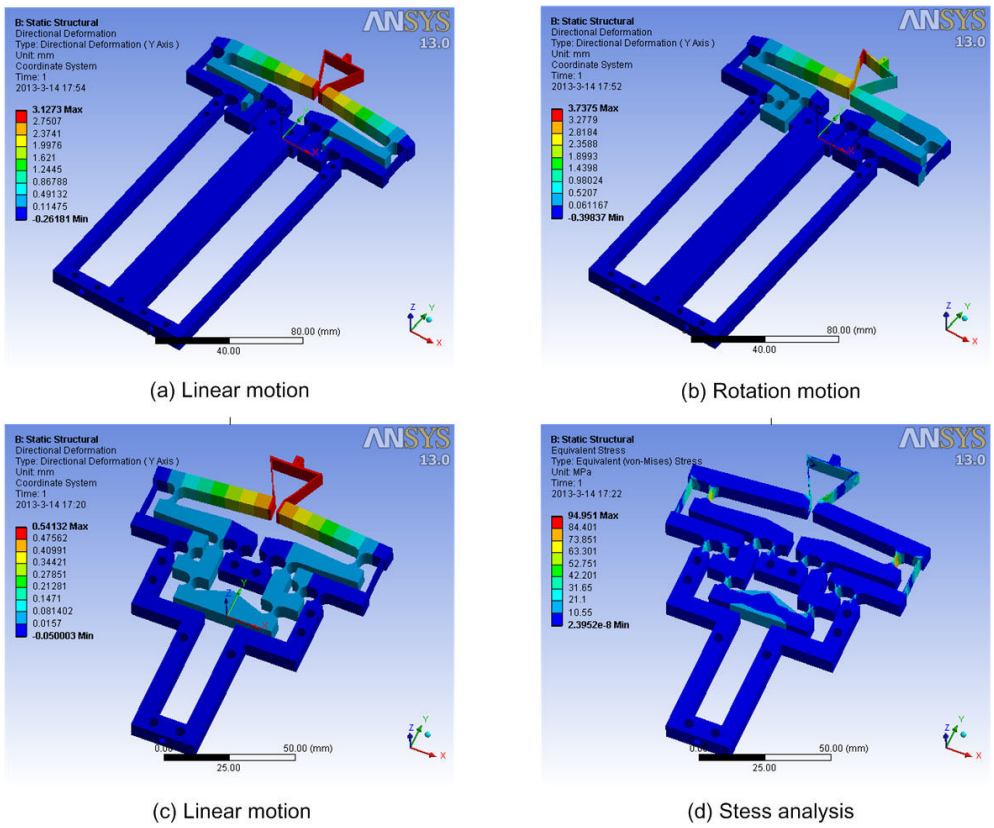

Fig. 7. The deformation shapes of the left and right micromanipulator. (a) Linear motion of the left-arm under the dual-load of 1300 N, (b) Rotation motion of the right micromanipulator under the maximum driven force 1800 N, (c) Linear motion of the right-arm with 30 μm, (d) Stress analysis result.

a better dynamics performance than the common steel or aluminum material.

An overview of the experimental setup is graphically displayed in Fig. 8. Two PZTs (model P-216.80 with open-loop travel of 120 μm and static large-signal stiffness of 50 N/μm $\pm$ 20, from PI, Inc.) are selected to drive the micromanipulator. One low-voltage (0-100 V) driven PZT (P-840.20 from PI, Inc.) with ultra-high open-loop motion resolution (0.3 nm) is employed to drive the right micromanipulator. Besides, two higher speed laser displacement sensors (model LTC-050-10, from MTI, Inc.) are adopted in this study. A dSPACE-1005 rapid prototyping system (from dSPACE GmbH) equipped with 16-bit DS2001 A/D and DS2102 D/A modular boards with the sampling frequency of 2 KHz are employed to implement the displacement amplification ratio tests. The output voltage signals of the dSPACE system (0-10 V) are amplified by a three-channel amplifier (E-464.00 from PI, Inc.), which generates an output voltage signal (0-1000 V) to drive the left two PZT actuators. A three-channel amplifier (E-503.00 from PI, Inc.), which generates a control voltage signal (0-100 V) to drive the right PZT. In the practical bio-manipulation experiments, the command signal and the output displacement data are generated and captured by the DAQ card (PCI-6289, from NI, Inc.) and the microscopy (Up-right BX51WI, from Olympus, Inc.) camera system (from TIS, Inc.), respectively. To avoid the trouble of vibrations, all the units except the dSPACE control system, and the host computer are mounted onto the high performance vibration isolation tables (from Olympus, Inc. and Thorlabs, Inc.).

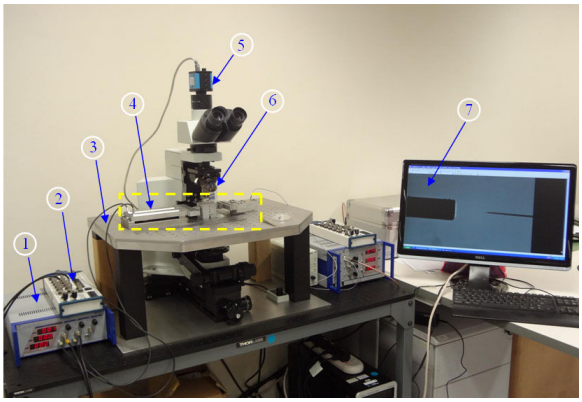

Fig. 8. The experimental setup of this study. (1) PZT amplifier, (2) BNC connector, (3) Vibration isolation stage, (4) The developed dual-arm flexure-based manipulators, (5) Camera system, (6) Microscopy system, (7) Host controlling computer.

B. Displacement Amplification Ratio and Workspace Tests

To characterize the dynamic properties of the fabricated micromanipulators, the experiments in terms of displacement amplification ratio and micromanipulator rotation angle tests are conducted in detail.

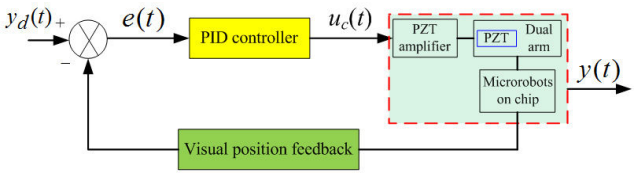

Fig. 9. Motion control strategy for the microrobots on chip.

Firstly, a periodic sine signal with a constant rate (20 μm/s) ranging from 0 to 1000 V is applied to the PZTs. By acquiring the input and output displacement, the actual lever displacement amplification ratio will be determined as 30.6 (the derivation is 7 %). Herewith, the displacement amplification ratio of the right micromanipulator is determined as 17.6 (the derivation is 2.8 %). Besides, in order to obtain the actual maximum mechanism rotation angle of the left mechanism, the input displacement and the lateral output displacement of end-effector are acquired simultaneously, then the maximum rotation angle of this micromanipulator can be calculated as around 26.5°. The total errors mainly arise from the preload effect of the PZT actuators, manufacturing, sensor noises, and assembly errors.

C. Bio-manipulation Experiment and Discussions

As a significant emerging model organism, zebrafish embryo is adopted and employed in our study. A microslide instead of the micro-fluidic chip is employed in this test. In the precision motion control process of the two microrobots, as shown in Fig. 9, the PID control strategy is utilized. The controlled plant consists of the PZT amplifier, dual-arm micromanipulators with the PZT actuators, and the microrobots driven by the magnetic forces. The image signal is captured and processed by the VC++ and Matlab software, feature recognitions are carried out and then control signal is generated and sent by the DAQ card to drive the PZT actuators, in which the "looking-then-moving" visual servo strategy is employed. Also, coordinate transformations are conducted between the image space and the practical microrobot spaces. The experimental processes are captured and demonstrated in Fig. 10.

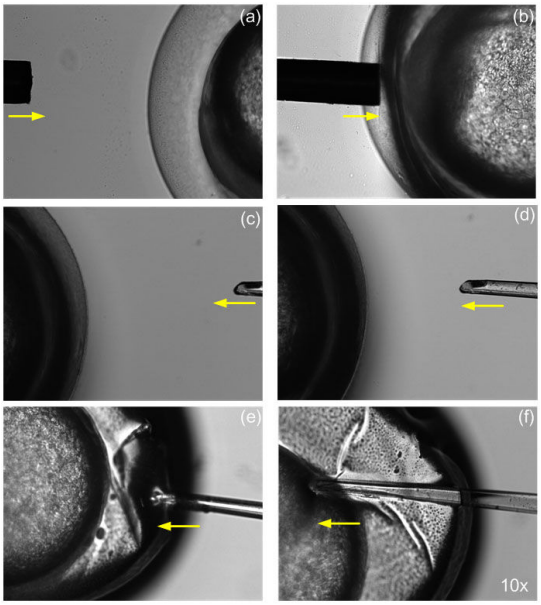

Fig. 10. The captured zebrafish embryo microinjection process. (a) The left microrobot goes ahead to grip the embryo, (b) The embryo is gripped by the microrobot, (c) The right microrobot with the micropipette goes ahead to inject the embryo, (d) The right microrobot with the micropipette is close to the embryo, (e) The micropipette is injected into the chorion. (f) The micropipette is injected into the yolk.

VI. Conclusion

A novel flexure-based dual-arm robotic system for performing biomanipulations on micro-fluidic chip is presented in this paper. Firstly, a novel biomanipulation method using flexure-based dual-arm robotic system is demonstrated. Then, a set of flexure-based large-workspace micromanipulator with modified differential lever displacement amplifiers is developed. Considering the practical requirements of large-workspace in biomanipulations, the dimension optimization by using the PSO algorithm is carried out. Also, the mechanism performance evaluation via ANSYS Workbench Platform is presented. Moreover, the prototype fabrication and the practical zebrafish embryo microinjection experiments are implemented in detail. The FEA and the experimental results uniformly prove that the developed compliant micromanipulator possesses a good performance for performing biomanipulations. Even so, how to acquire the force between the end-effector and the cells is a significant issue, it will be used to avoid the trouble of cell damage, which will be conducted in our future work.

References

[1] G. J. Lieschke and P. D. Currie, "Animal models of human disease: zebrafish swim into view," *Nature Reviews Genetics*, vol. 8, pp. 353-367, 2007.

[2] T. I. Brelidze, A. E. Carlson, B. Sankaran and W. N. Zagotta, "Structure of the carboxy-terminal region of a KCNH channel", *Nature*, vol. 481, pp. 530-533, 2012.

[3] J. K. Kim, I. Hwang, D. Britain, T. D. Chung, Y. Sun, and D.H. Kim, "Microfluidic approaches for gene delivery and gene therapy," *Lab on a Chip*, vol. 11, pp. 3941-48, 2011.

[4] C. Pawashe, S. Floyd, and M. Sitti, "Multiple magnetic microrobot control using electrostatic anchoring," *Appl. Phys. Lett.*, vol. 94, pp. 164108-1-164108-3, 2009.

[5] M. Hagiwara, T. Kawahara, Y. Yamanishi, T. Masuda, L. Feng, and F. Arai, "On-Chip magnetically actuated robot with ultrasonic vibration for single cell manipulations", *Lab on a Chip*, vol. 11, no. 12, pp. 2049-2054, 2011.

[6] M. Hagiwara, T. Kawahara, Y. Yamanishi, and F. Arai, "Driving method of microtool by horizontally arranged permanent magnets for single cell manipulation," *Appl. Phys. Lett.*, vol. 97, pp. 013701-1-013701-3, 2010.

[7] Y. Li, J. Huang, and H. Tang, "A compliant parallel XY micro-motion stage with complete kinematic decoupling," *IEEE Trans. Auto. Sci. Eng.*, vol. 9, no. 3, pp. 538-553, 2012.

[8] H. Tang, Y. Li, and J. Huang, "Design and analysis of a parallel XY micromanipulator for micro/nano manipulation driven by dual-mode," *Proc. Inst. Mech. Eng., Part C, J. Mech. Eng. Sci.*, vol. 226, no. 12, pp. 3043-3057, 2012.

[9] W. H. Wang, X. Y. Liu, and Y. Sun, "High-throughput automated injection of individual biological cells," *IEEE Trans. Auto. Sci. Eng.*, vol. 6, no. 2, pp. 209-219, 2009.

[10] H. Tang and Y. Li, "Design, analysis and test of a novel 2-DOF nanopositioning system driven by dual-mode," *IEEE Trans. Robot.*, vol. 29, no. 3, pp. 650-662, June 2013.